AD-A032 374 AIR FORCE GEOPHYSICS LAB HANSCOM AFB MASS F/G 4/2
EXPERIMENTAL STUDIES OF THUNDERSTORM ELECTRIFICATION.(U)
JUN 76 D R FITZGERALD
UNCLASSIFIED AFGL-TR-76-0128 NL

1 OF 1
AD A032374

END

DATE FILMED
1-77

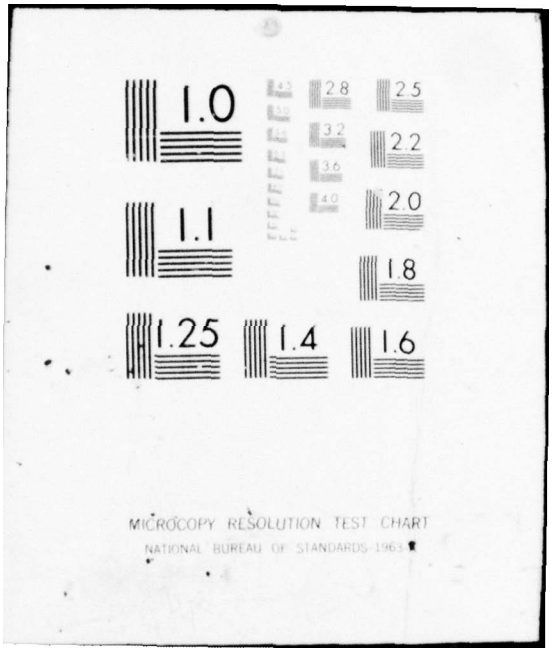
1.0
2.8
2.5
3.2
2.2
3.6
2.0
4.0
1.1
1.8
1.25
1.4
1.6
MICROCOPY RESOLUTION TEST CHART
NATIONAL BUREAU OF STANDARDS-1963

AFGL-TR-76-0128
ENVIRONMENTAL RESEARCH PAPERS, NO. 567

(12)
NW

Experimental Studies of Thunderstorm Electrification

DONALD R. FITZGERALD

22 June 1976

METEOROLOGY DIVISION PROJECT 8620
AIR FORCE GEOPHYSICS LABORATORY
HANSCOM AFB, MASSACHUSETTS 01731

AIR FORCE SYSTEMS COMMAND, USAF

This technical report has been reviewed and is approved for publication.

FOR THE COMMANDER:

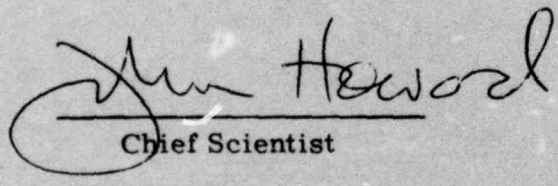

Chief Scientist

Qualified requestors may obtain additional copies from the Defense Documentation Center. All others should apply to the National Technical Information Service.

Unclassified

SECURITY CLASSIFICATION OF THIS PAGE (When Data Entered)

REPORT DOCUMENTATION PAGE	READ INSTRUCTIONS BEFORE COMPLETING FORM
1. REPORT NUMBER: AFGL-TR-76-0128, AFGL-ERP-567	2. GOVT ACCESSION NO. / 3. RECIPIENT'S CATALOG NUMBER
4. TITLE (and Subtitle): EXPERIMENTAL STUDIES OF THUNDERSTORM ELECTRIFICATION,	5. TYPE OF REPORT & PERIOD COVERED: Scientific. Final rept.
	6. PERFORMING ORG. REPORT NUMBER: ERP 567
7. AUTHOR(s): Donald R. Fitzgerald	8. CONTRACT OR GRANT NUMBER(s)
9. PERFORMING ORGANIZATION NAME AND ADDRESS: Air Force Geophysical Laboratory (LYC) Hanscom AFB, Massachusetts 01731	10. PROGRAM ELEMENT, PROJECT, TASK AREA & WORK UNIT NUMBERS: 61102F 86200101
11. CONTROLLING OFFICE NAME AND ADDRESS: Air Force Geophysical Laboratory (LYC) Hanscom AFB, Massachusetts 01731	12. REPORT DATE: 22 June 1976
	13. NUMBER OF PAGES: 40
14. MONITORING AGENCY NAME & ADDRESS (if different from Controlling Office)	15. SECURITY CLASS. (of this report): Unclassified
	15a. DECLASSIFICATION/DOWNGRADING SCHEDULE

16. DISTRIBUTION STATEMENT (of this Report)

Approved for public release; distribution unlimited.

17. DISTRIBUTION STATEMENT (of the abstract entered in Block 20, if different from Report)

16 8620 17 01

18. SUPPLEMENTARY NOTES

19. KEY WORDS (Continue on reverse side if necessary and identify by block number)

Aircraft measurements
Atmospheric electric fields
Thunderstorm measurements
Lightning

20. ABSTRACT (Continue on reverse side if necessary and identify by block number)

Airborne electric field sensing and computing systems have been developed and flown on C-130, F-100F, RF4C, and U-2 aircraft for studies of shower, cloud, and thunderstorm charge centers. Examples are given of the proper separation of field components and aircraft charge during thunderstorm penetrations and during direct lightning strikes to the test aircraft. Techniques have been employed for roll compensation of the aircraft-fixed field → next page

DD FORM 1 JAN 73 1473 EDITION OF 1 NOV 65 IS OBSOLETE

Unclassified

SECURITY CLASSIFICATION OF THIS PAGE (When Data Entered)

409578

20. (Cont)

cont.

components so that real-time vector displays indicating the centroid of near-by charge concentrations are available for use in avoidance of probable lightning areas, or for use in selecting them to maximize the probability of a strike to test aircraft during lightning-aircraft interaction studies.

The development of the storm electrical structure is directly related to details of the cloud water and ice distribution linked through the thermal and draft structure in the storm. Major features of the internal electrical pattern are often seen in data taken above, alongside, or at the surface. However, in accordance with electrostatic field theory, many of the fine structural details found within the storm are suppressed outside. The major vertical component field pattern is found to be one that could be produced by simple tilted dipolar charge structures. Depending on the physical conditions in different regions of the storm, the upper excess charge of the dipole may be either positive as generally reported from surface observations of the field, or it may be negative, as found in a number of the U-2 storm overflights accomplished in this project.

Preface

The aircraft instrumentation and operational mode employed in these tests were developed as elements of the Rough Rider project, in a joint effort of National Weather Service severe storms research activities; the Adverse Weather Branch; Aeronautical Systems Division, AFSC; and AFGL. Specialized additional support to the lightning measurement phase of the program was provided by AFWL, Sandia Laboratories, and the Federal Aviation Administration. Dr. Robert M. Cunningham and Lt Col. J. F. Church of AFGL provided considerable assistance to the flight measurement and aircraft coordination aspects of the program.

Contents

Illustrations

Tables

Experimental Studies of Thunderstorm Electrification

1. INTRODUCTION

The research on thunderstorm cloud physics conducted in Project 8620 was directed toward an understanding of the number of complex interactions that occur in the development of electrical charge centers and lightning activity in showers and thunderstorms.

The original thunderstorm project conducted by Professors Byers and Braham[1] utilized extensive mesoscale surface meteorological networks, radar observations, and up to five aircraft penetrating storms in Ohio and central Florida. The results of this study led to major advances in the understanding of thunderstorm draft, precipitation, and thermal structure. However, flights were limited to altitudes of 26,000 ft, or below, and severe difficulties were encountered in obtaining reliable electrical measurements from the aircraft during storm penetrations.

The present study was initially developed to improve the techniques for electrical measurements in storms and to extend the measurements to higher altitudes in and around storms. These techniques represent an extension of the work of the Army-Navy Precipitation Static Project under Ross Gunn et al[2]; the Cornell

(Received for publication 17 June 1976)

1. Byers, H.R. and Braham, R.R. (1949) The Thunderstorm, U.S. Govt. Printing Office, Washington, D.C.

2. Gunn, R., et al (1946) Army-Navy precipitation static project, Proc. Inst. Radio Eng. 34:156 and 34:234.

Aeronautical Laboratory work of S. Chapman;[3] and the Naval Research Laboratory work of J. F. Clark and associates.[4]

A very active flight program was conducted during the time period 1961 to 1966 utilizing three well instrumented aircraft: A U-2, a C-130, and a F-100F. Voluminous data, mostly in the form of oscillographic paper records and film, were acquired from coordinated flights in Oklahoma and central Florida.

Short reports on aspects of the data have been presented by Fitzgerald[5-9] and Fitzgerald and Cunningham.[10] Various diversions of the analysis personnel to work on other applied Air Force problems, and the inherent complexity of the phenomena have resulted in slow progress. However, the recent acquisition and use of appropriate data reduction equipment has led to considerable advances in interpretation of the strongly time and position dependent field data and of the interrelations with other features of the storms.

This report summarizes the instrumentation developed and indicates the electrostatic characteristics of the aircraft used in the program. It is shown that reliable aircraft electrical measurements can be made during thunderstorm penetrations. Some examples are given of the interpretation of the electrical data in relation to storm draft, turbulence, and precipitation features. Refinements of these concepts may lead to practical airborne lightning avoidance instruments and to improved techniques of IFR flights in thunderstorm areas.

---

3. Chapman, S. (1955) Discharge of Corona Current from Points on Aircraft or on the Ground, Report CAL66. Cornell Aeronautical Laboratory, Inc. Buffalo, N.Y.

4. Clark, J. F. (1957) Airborne measurements of atmospheric potential gradient, J. Geophys. Res. 62:617.

5. Fitzgerald, D.R. (1965) Measurement techniques in clouds, in Problems of Atmospheric and Space Electricity, ed. S.C. Coroniti, Elsevier Publishing Co., Amsterdam.

6. Fitzgerald, D.R. (1967) Probable aircraft triggering of lightning discharges in certain thunderstorms, Mo. Wea. Rev., 95:835.

7. Fitzgerald, D.R. (1968) USAF flight lightning research, in Proc. Conf. on Lightning and Static Electricity, 3 to 5 Dec 1968. AFAL TR-68-0290, DDC - AD 693135.

8. Fitzgerald, D.R. (1970) Aircraft and rocket triggered natural lightning discharges, in Proc. Lightning and Static Electricity Conf., Soc. of Auto Engrs, N.Y.

9. Fitzgerald, D.R. (1974) Electrical structure of large overwater shower clouds, in Electrical Processes in Atmospheres, ed. by H. Dolezalek and R. Reiter, Dietrich-Steinkopff, Darmstadt, Germany (in press).

10. Fitzgerald, D.R. and Cunningham, R.M. (1965) Multiple aircraft studies of the electrical properties of thunderstorms, in Proc. Intl. Conf. on Cloud Physics, Tokyo and Sapporo, Japan.

2. ELECTROSTATIC FIELD MEASUREMENT TECHNIQUES FOR HIGH PERFORMANCE AIRCRAFT

2.1 Sensor Characteristics

The development of regions of cloud electric charge can be monitored by suitable electrostatic field sensors. These sensors may be used in pairs to measure a voltage difference between two points, separated by a distance d, which can be interpreted as V/d = E, the average electric field; or an induction technique may be used directly to measure the field at a point.

Measurement of voltage is usually done with a high impedance or radioactive probe. The direct field measurement can be done by chopping the field lines with a relatively low impedance field "mill" to generate an AC signal of amplitude proportional to the incident field strength. Potential measurements can be made to weaker field levels because of the residual mechanical noise signal associated with field mills; however, the decreased sensitivity of field mills to weather effects and probable better performance in high field conditions suggest that field mills will provide better results if power and weight limitations are not critical. Therefore, field mills were selected for use in these aircraft experiments. A typical mill, as used on the F-100F, is shown in Figure 1. Field mills have been used for electrostatic measurements since the 1920's. A review of their operation was provided by Waddell[11] and Mapleson and Whitlock.[12] The basic technique for a flat plate-type mill is to alternately shield and expose an insulated conductor (stator) to the ambient field through use of a movable, grounded, conducting cover plate (rotor). The charge induced on the stator is coupled through a parallel RC network into an AC amplifier. A cyclical flow of charge through the network to the stator and back to system ground occurs as the stator is unshielded and shielded by the rotor. This produces the basic signal. Most field mills also provide a reference signal generator to produce a fixed AC signal which is in or out of phase with the incident field signal. These signals are combined in a balanced detector circuit to obtain a DC output with amplitude proportional to the incident field strength, and positive or negative polarity in correspondence with the sign of the incident field.

---

11. Waddel, R.C. (1948) An electric field meter for use on airplanes, Rev. Sci. Instr., 19:31.
12. Mapleson, W.W. and Whitlock, W.S. (1955) Apparatus for the accurate and continuous measurement of the earth's electric field, J. Atmos. Terr. Phys. 7:61.

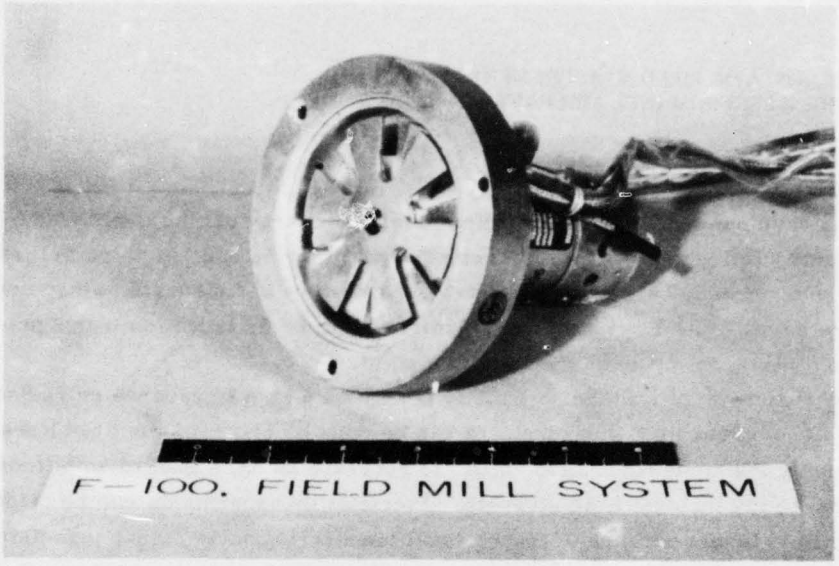

Figure 1. F-100F/U-2 Field Mill

If field mills of this type are connected in a circuit whose input resistance $R >> 1/\omega C$, where C is the average input capacitance, then the theoretical ac signal voltage available is given by

$$V_{peak} \simeq (\epsilon_o A_o / 2C)\, E .$$

A_o is defined as the maximum stator area exposed to the incident field E. C is normally selected as between 500 and 1000 pf. Stator areas for feasible aircraft sensors are in the range 10 to 100 cm^2. The actual signal frequency is determined by the product of the rotor driving motor speed in rps and number of rotor/stator metallic segments used in the mill construction. Field fringing effects normally reduce the mill output to values less than given by the above equation.

An alternate to the flat plate field mill is a cylindrical one in which the isolated conducting segments on the surface of a cylinder are rotated about an axis perpendicular to the direction of the incident field to be measured. Refinements to this type device have been discussed by Kasemir[13, 14] and several of this type have been installed and operated on relatively slow aircraft. These units have a

13. Kasemir, H. W. (1951) Die Feldkomponentenmuhle Tellus 3:240.
14. Kasemir, H. W. (1964) The Cylindrical Field Mill, US Army Electronics Command, TR ECOM-2526, Fort Monmouth, N. J. (DA Task No. 1VO-14501-B-53A-11).

disadvantage of protruding a significant distance above the aircraft skin, thus adding drag. It also appears likely that they could suffer signal degradation in precipitation and icing conditions. They have a significant advantage of automatically cancelling out effects of the field due to local aircraft charge since the signal pickup electrodes are operated in a differential mode and are rotating symmetrically with respect to the charged aircraft skin.

The sensors used in this project were all of the flat plate configuration. Symmetrical mountings on the various aircraft were used to simplify the compensation for aircraft charging effects.

2.2 Siting Considerations

The geometric shape of an aircraft causes the local electric charge density to vary considerably with position on the aircraft. This charge density is composed of a component, σ_1, due to the net charge on the aircraft and to another σ_2, due to the charges induced on the airframe by any external electric fields in the vicinity.

Ideally the sensors should be placed so that discrimination against unwanted field components is maximized. Field mapping techniques using models of the aircraft in question can be used as an aid in selecting optimum positions.

If two of the sensors can be mounted at locations of symmetry with respect to an external field component, which are locations also of equal aircraft net charge density, the external and aircraft field values can be separated by simple addition and subtraction of the two sensor's output values.

For flight measurements in a variety of IFR conditions it is desirable to use flush mounted sensor housings with the sensitive elements slightly recessed. Installations should keep the sensor face parallel to the local airflow so that there will be no particle impingement or icing of the sensor. The input impedance levels should also be relatively low to minimize leakage effects across the stator insulation.

2.3 Applications to Project Aircraft

2.3.1 C-130 SYSTEM

The basic C-130 aircraft field meter system has been developed to provide measurement of the x, y, and z electric field components associated with cloud charge distributions and to provide a measurement of the charge on the aircraft.

The system utilizes four electric field meters of the induction type. These meters face outward from the aircraft in the location FM shown on Figure 2. They are contained within metallic housings that have a motor-driven cover plate so that the meters can be enclosed for protection from weather and other hazards until airborne. The cover plate may also be actuated in flight to provide a zero field

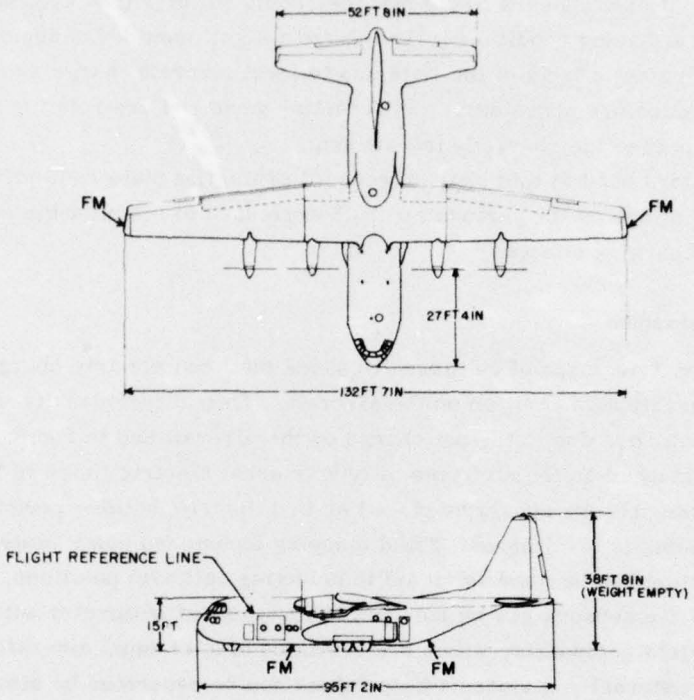

Figure 2. C-130A Field Sensor Locations

condition on each meter individually for flight test checks of the system performance. A block diagram of the whole equipment is shown in Figure 3. In the original system, ac signals of amplitude proportional to the field intensity at each meter were transmitted through a cathode follower over a coaxial cable to the computer and recorder units located in the rear fuselage area. A reference-signal generator in each head provided a signal used for determination of the polarity of the incident field and for an inflight check of system gain stability.

Amplification of the ac signal and reference voltage was followed by phase detection, resulting in a dc signal from each channel with positive or negative polarity, depending on the sign of the incident field.

In the latest version, completed in 1974, the ac and reference signals are combined in the sensor head electronic package, and only the dc signal is sent into the computer.

The measured electric field components are defined in a downward-pointing right-hand coordinate system selected for ease of analysis of charged-cloud structure.

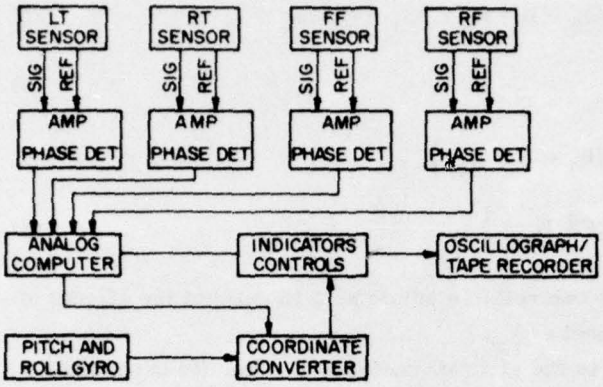

Figure 3. C-130A Field Meter System Block Diagram

In this system a positive field direction is taken as the direction a positive charge will move in the field. The axes are centered on the aircraft with plus E'_x directed longitudinally along the fuselage toward the tail; plus E'_y is along the wing span from the right wing toward the left wing; and plus E'_z is directed downward. Plus E_q denotes a positive surface charge on the aircraft.

The dc output voltages from the right tip, left tip, forward fuselage, and rear fuselage are related to the field components by the following equations:

$$V_{rt} = S_{rt} \, (AE'_y - E_{qw}) , \tag{1}$$

$$V_{lt} = S_{lt} \, (-AE'_y - E_{qw}) , \tag{2}$$

$$V_{ff} = S_{ff} \, (C_1 E'_x - B_1 E'_z - E_{qff}) , \tag{3}$$

$$V_{rf} = S_{rf} \, (-C_2 E'_x - B_2 E'_z - E_{qrf}) , \tag{4}$$

where S represents the sensitivity of the channel in volts per volt/cm applied field and V is the dc voltage from the detector.

The dc signals are then fed into an analog computer. This unit performs addition and subtraction operations to yield outputs proportional to the aircraft charge and to the components of the external field vector with respect to the coordinate system defined by the instantaneous aircraft axes. These outputs, to the first order effects, are as follows:

$$V_q = 2\overline{S}_q \, E_{qw} , \tag{5}$$

$$V_x = \bar{S}_X \left\{ (E_{q_{rf}} - E_{q_{ff}}) + (B_2 - B_1) E'_z - (C_1 + C_2) E'_x \right\} , \quad (6)$$

$$V_y = -2\bar{S}_y A E'_y , \quad (7)$$

$$V_z = \bar{S}_z \left\{ (C_2 - C_1) E'_z + (B_1 + B_2) E'_z \right\} ,$$

$$+ S_z \left\{ (E_{qff} + E_{qrf}) - 2F\bar{S}_q E_{qw} \right\} . \quad (8)$$

where F in Eq. (8) is an in-flight controllable adjustment to null out the effects of aircraft charge on the measurement of V_z.

Neglecting difference terms in the aircraft coefficients, Eq. (6) becomes

$$V_x = -\bar{S}_x (C_1 + C_2) E'_x . \quad (9)$$

When the value of F in Eq. (8) is adjusted in flight so that V_z is independent of changes in the aircraft charge, Eq. (8) may be written

$$V_z = \bar{S}_z (B_1 + B_2) E'_z . \quad (10)$$

The voltages indicated in Eqs. (5), (7), (9), and (10) are used to operate meters for visual indication of field effects and also are routed to recorder channels through appropriate scaling resistors. A ground calibration of the whole system is achieved by applying known fields to calibration plates attached to the input sensors and relating these to recorder trace deflections.

A gyro-controlled coordinate transformation system has been installed to convert the E'_y and E'_z channel outputs from the aircraft axes to roll-stabilized axes so that the E_y and E_z components are horizontal and vertical respectively, whether or not the aircraft is in level flight.

A final computation state involves rectangular-to-polar coordinate converters so that the direction and magnitude of the field vector in the three coordinate planes can be seen in flight and used to alter course as required to investigate the indicated charge centers or to avoid probable areas of lightning or static-discharge activity.

2.3.2 F-100F SYSTEM

The electronics for the input stages of this system were fabricated using subminiature vacuum tubes and ruggedized construction since the intent was to make thunderstorm penetrations and obtain data on the characteristics of lightning strikes to the aircraft. The fuselage structure made it impracticable to locate two sensors on the lower fuselage. The three sensors used were positioned as shown in

Figure 4. The actual configurations used are shown in Figures 5 and 6, since a similar arrangement could be applied to other aircraft. The electronics package shown in Figure 7 was mounted in a left gun bay.

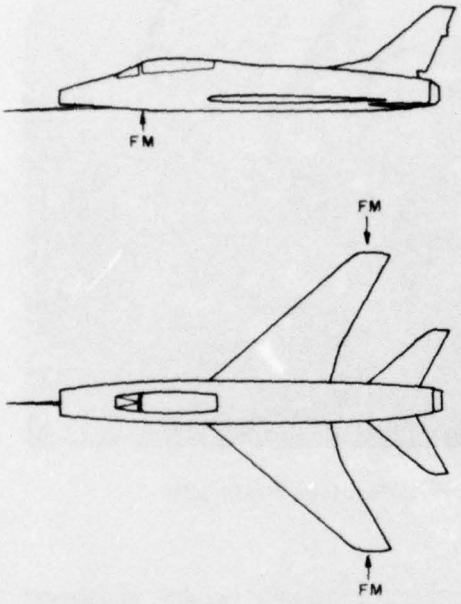

Figure 4. F-100F Field Sensor Locations

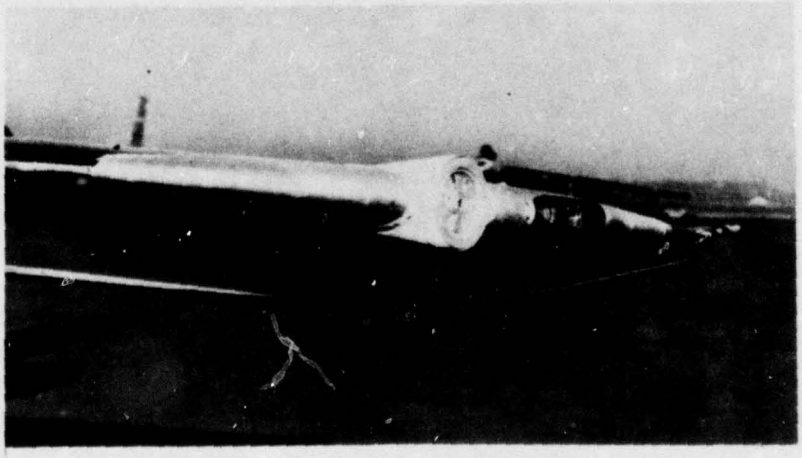

Figure 5. F-100F Wing Tip Field Mill

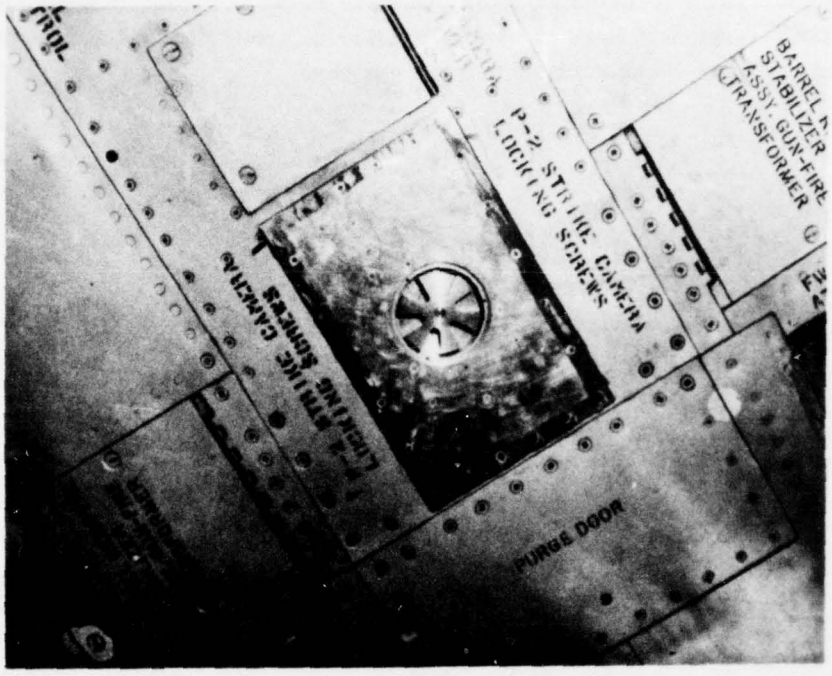

Figure 6. F-100F Lower Fuselage Field Mill

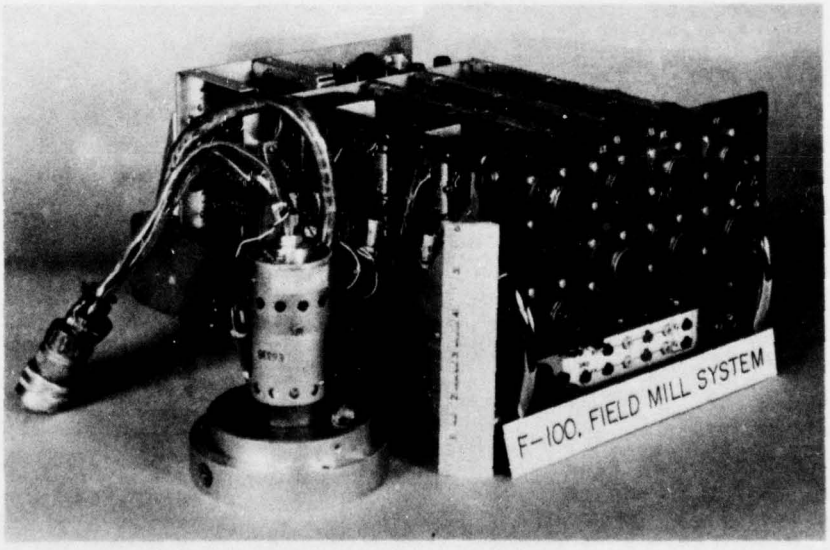

Figure 7. F-100F Electronics Assembly

With three sensors as positioned, it is not possible to measure the field component E_x along the flight direction. However, E'_y, E'_z, E_q can be determined in the same manner as described for the C-130 installation.

2.3.3 U-2 SYSTEM

The initial U-2 system used from 1961 to 1963 included a modified two channel amplifier similar to that described by Clark,[4] and a top and bottom fuselage mounted field mill in the equipment bay areas to the rear of the cockpit. A field strength indicating meter and 10 position range switch was installed for pilot use. The system was revised in early 1964 and configured in the same general manner as the F-100 system except that more gain was used in the ac amplifiers since fields to be measured above storms were weaker than those expected in the storm. It was impracticable to use wingtip sensors, so the two side-facing units were mounted symmetrically on the sides of the engine inlet fairings, as shown in Figure 8. The lower fuselage sensor was mounted near the nose of the aircraft. The fuselage shape in this area can be readily approximated by an ellipsoid, so it was possible to make good calculations of the external field augmentation factors at this location.

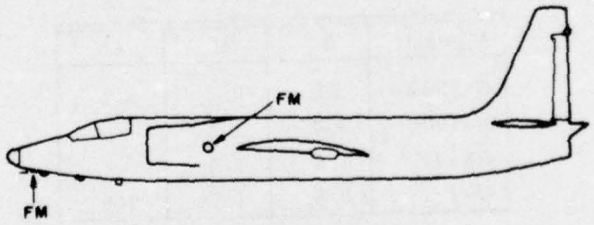

Figure 8. U-2 Field Sensor Locations

2.3.4 RF4C SYSTEMS

The U-2 and F-100F systems were recently refurbished and installed on RF-4C aircraft to provide high altitude electrical measurements in support of the Apollo-Soyuz Test Program. The horizontal sensors were installed facing outwards on both sides of the fuselage, ahead of the engine inlets. The vertical sensor was on the lower fuselage center line in the same vicinity. The electronics were nearby in a forward equipment bay. Data readouts were provided to meters installed in the rear cockpit.

2.4 Field Augmentation Considerations

The introduction of a conducting body, such as an aircraft, into a region of space containing an electric field will distort the field lines. The field will be concentrated in a non-uniform manner, with the largest field intensities occurring on the regions of smallest radius of curvature, such as pitot boom tips and wing tips. Thus, in order to measure the ambient "true" field from the aircraft, it is necessary to compensate for this field augmentation effect. The irregular shapes of aircraft and the fact that the measured fields at a particular site will depend both on the large-scale distortion and on local details of the housing and sensor geometry make it unwise to rely on theoretical electrostatic calculations for the final evaluation of the augmentation factors.

In this program theoretical calculations using cylindrical and ellipsoidal models to approximate portions of the airframes were made. The large scale, clear air, field patterns of thunderstorms were used to cross calibrate relative augmentation factors through a series of formation flights. Laboratory measurements were also made of localized sensor housing augmentations. A best fit combination of the above techniques was then used to assign numerical values for each aircraft. The factors determined are shown in Table 1.

Table 1. Sensor Housing Augmentations

Aircraft	A	B	C
C-130A	21	2.2	5.5
F-100F	8.8	1.1	--
RF-4C	1.5	1.4	--
U-2	0.6	1.7	6.8

In the above, A is the factor for the field component along the wing span, B is the factor for the lower fuselage augmentation of the vertical field component, and C is the factor for the lower fuselage augmentation of the component along the fuselage. This factor changes greatly with position of the sensor on the fuselage. An illustration of one check of the F-100F values is given in Figure 9. The flight was conducted below a thunderstorm cloud base over the ocean, off Cape Canaveral, Florida. The true field was believed to be largely vertical. High angle banks were used to maintain the desired flight pattern, thus resulting in both E_y' and E_z' data values. When the roll stabilization equations seen in the figure were applied, the true field was confirmed to be vertical. Flight data electric fields given in this report have been corrected in accordance with the factors listed.

F-100F SAMPLE CALCULATION: FIELD COMPONENTS AND FORM FACTOR CHECK

1. ROLL TRANSFORMATION EQUATIONS (NO PITCH)

$$E_y = E'_y \cos\beta - E'_z \sin\beta$$

$$E_z = E'_y \sin\beta + E'_z \cos\beta$$

Figure 9. F-100F Low Altitude Augmentation Factor Check

2. DATA

PASS 2 5 SEC BEFORE LIGHTNING; IN 59 DEG LEFT TURN

$AE'_y = -2440$ V/CM $A = 8.8$ $E'_y = -278$ V/CM

$BE'_z = -185$ V/CM $B = 1.1$ $E'_z = -168$ V/CM

APPLYING EQUATIONS: $E_y = -143 + 144 \approx 0$

$E_z = -238 - 86 = -324$ V/CM

3. THUNDERSTORM FIELD DATA

3.1 Operations and Instrumentation

The C-130, F-100F, and U-2 normally attempted to fly joint coordinated passes around, through, and over selected thunderstorms during the lightning test phase of the Rough Rider project. FAA controllers were detached to the project to arrange air space clearances and most importantly to exercise detailed control of the test aircraft in real time so that the aircraft could line up and be working the same area of the same storm.

Ground and C-130 aircraft radar displays were photographed for each storm and on-board cameras were used for cloud structure documentation from each aircraft. In addition to the electric field measurements, a number of other flight data and cloud physics parameters were obtained. Temperature and acceleration data were available from all aircraft. The F-100F had additional gust vane, height change, pitch, and elevator position measurements so that gust and draft calculations could be made. The U-2 had a downward looking, 8 to 13 micron, infrared system with a two degree field of view for storm top temperature measurements. The data were linked through the Eastern Test Range time code transmissions recorded on all aircraft.

3.2 Validity of In-Storm Data

A primary concern of the investigators of thunderstorm electrification has been the validity of data acquired within storms. Water, either as droplets or ice forms, is well known for its propensity to separate electrical charges upon impact with aircraft or rocket surfaces, thus possibly distorting or invalidating measurements of ambient field patterns. In addition, the high field conditions or surface charging of the test vehicle by particle impact, may result in corona currents from high curvature locations which might affect the measurements.

The symmetrical locations and flush mountings of field mills as used in this program are believed to have substantially reduced the influence of such effects on the measurements to be described. A good check on symmetry balance and decoupling of the field components from the aircraft charge is provided by examination of the transient field data obtained during lightning strikes to the aircraft. An example of the analog magnetic tape playback for a strike to the F-100F is shown in Figure 10. The top traces is the vertical field, the horizontal is in the center, and charge is at the bottom of the figure. It is seen that the horizontal component of field was largely unaffected by this strike and that the aircraft charge undergoes large excursions without affecting the external field components.

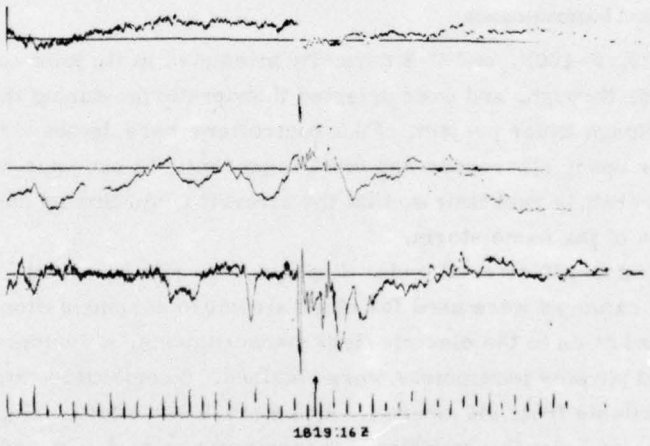

Figure 10. Decoupling of Field Components During Lightning Strike

The effects of corona on the measurements is manifested by small sawtooth modulation of a data channel. The amplitude of the field is not greatly affected by the corona and it is easily possible to interpolate a static field value through the zone of disturbance.

Corona events were rarely encountered during the series of storm flights. The aircraft was equipped with a number of wick discharges and had curved aluminum rods projecting about 50 cm to the rear of the wingtips as part of the lightning current measurement systems. These items would all act to distribute the main corona currents symmetrically to the rear in the aircraft wake, thus having little effect on the transverse field measurement.

3.3 General Character of Thunderstorm Field

3.3.1 SURFACE AND LOW ALTITUDE CONDITIONS

Surface measurements from point observations or networks of electric field sensors indicate complex but rather systematic alterations of field as storms develop near or move by particular locations. The field intensity and the duration or occurrence of zones of field directional reversals will depend on the intensity of the draft structure; on the in-cloud and sub-cloud precipitation patterns; their locations with respect to the field observation point; and on the storm cloud development and translation in response to the atmospheric wind pattern.

In view of present interests in using the earth's electric field for various inexpensive RPV and missile attitude sensing techniques, several examples of data, acquired in this and a previous study of storms will be given to illustrate typical features of the storm pattern near the ground. The following group of seven figures, reproduced in part from Fitzgerald,[15] are from a radar and eight station surface field meter network study conducted near the University of Illinois airport with the assistance of the Illinois State Water Survey.

Figures 11 and 12 indicate single station data on typical patterns associated with fairly weak convective clouds passing near the station. Figure 13 illustrates amplitude and phase differences in field maxima and minima observed when the time series data of four stations were combined. A multi-pole analysis for charge groupings above a conducting plane representing the earth's surface was carried out. The monopole and dipole terms lead to an expression for the vertical field component as seen in Figure 14. The resulting pattern on the earth is seen in Figure 15 for a particular tilted charge distribution and cloud motion that approximates the observed data of Figure 13. The theoretical time series is seen in the lower portion of Figure 13. Apparently complex field patterns can frequently be approximated by a model consisting of a number of these separate tilted dipolar charge clusters each imbedded in or near the edge of cloud precipitation radar echoes and moving past the observation point in accordance with the cloud-level wind field. Generally similar patterns are found during cloud penetrations and in the clear air above storms.

15. Fitzgerald, D. R. (1957) Some theoretical aspects of the relation of surface electric field observations to cloud charge distributions, J. Met., 14:505.

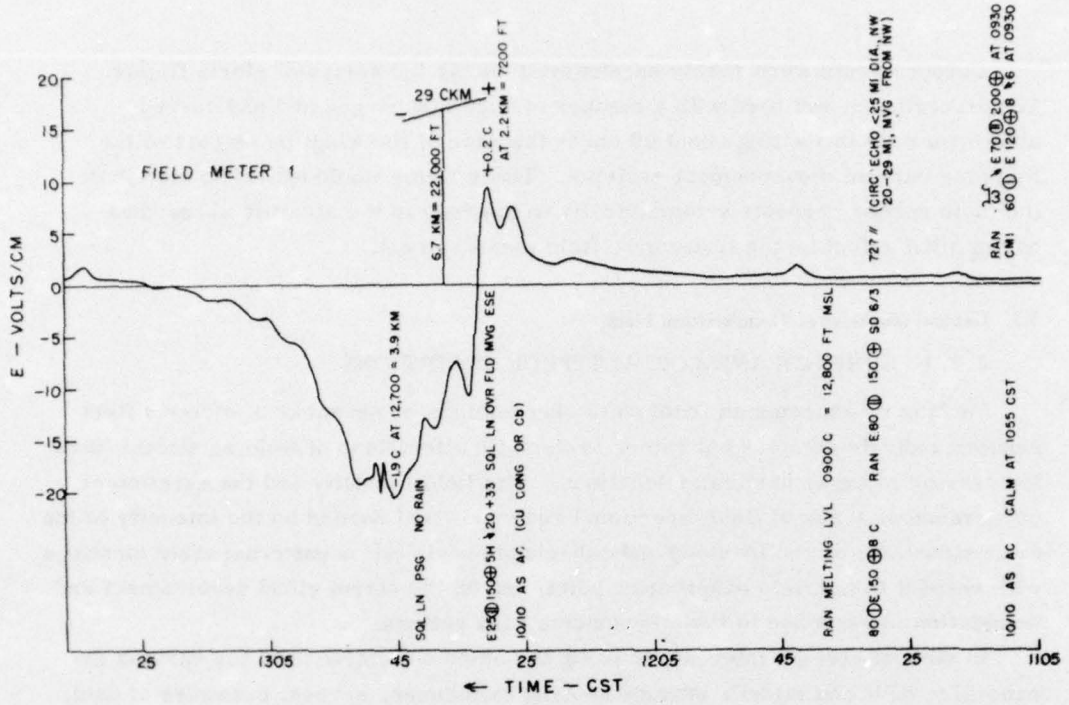

Figure 11. Surface Field With Weak Squall Line Passage

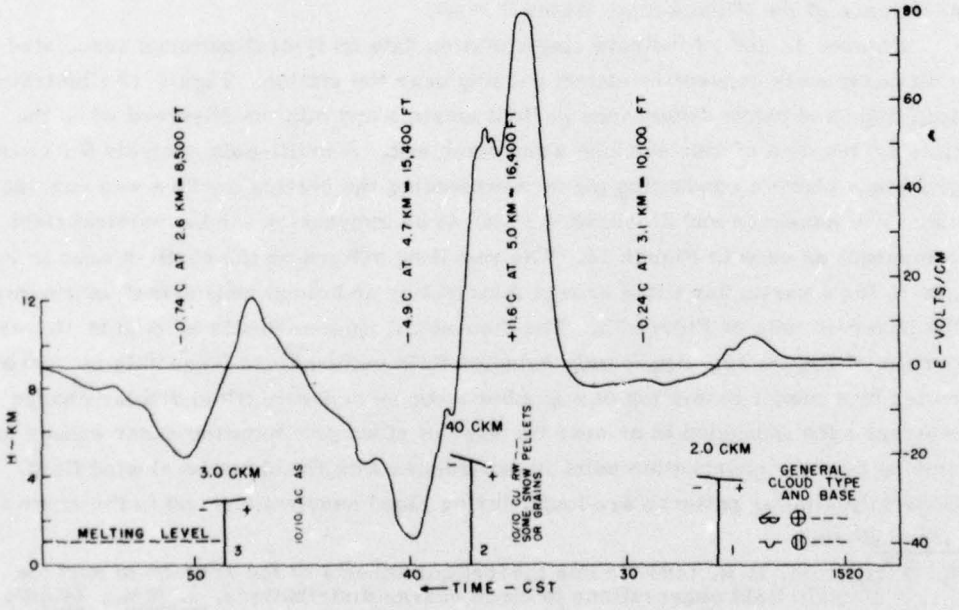

Figure 12. Surface Field With Snow Showers

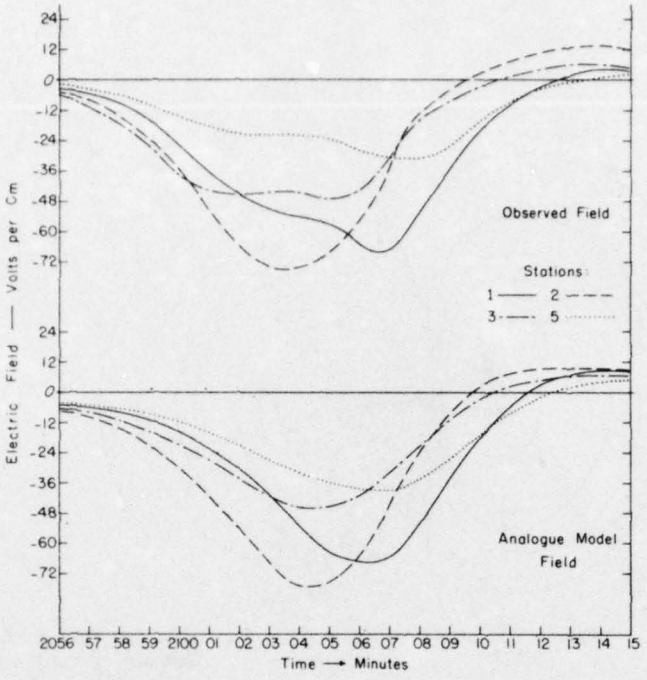

Figure 13. Agreement of Observed and Theoretical Surface Field Pattern

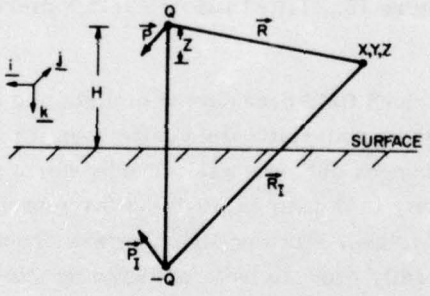

$$4\pi\epsilon_0\phi(X,Y,Z) = Q\left(\frac{1}{R} - \frac{1}{R_I}\right) + \frac{\vec{R}\cdot\vec{P}}{R^3} - \frac{\vec{R_I}\cdot\vec{P_I}}{R_I^3}$$

$$\vec{R} = X\underline{i} + Y\underline{j} + Z\underline{k} \qquad \vec{R_I} = X\underline{i} + Y\underline{j} - (2H - Z)\underline{k}$$

$$\vec{P} = \int_V \rho(X'\underline{i} + Y'\underline{j} + Z'\underline{k})dV \qquad \vec{P_I} = \int_{V_I} \rho(X'\underline{i} + Y'\underline{j} - Z\underline{k})dV$$

$$E_Z = \frac{3H}{2\pi\epsilon_0 R^5}\left[\frac{R^2 Q}{3} + XP_X + YP_Y + H\left(1 - \frac{R^2}{3H^2}\right)P_Z\right]$$

Figure 14. Electric Field Equation Development

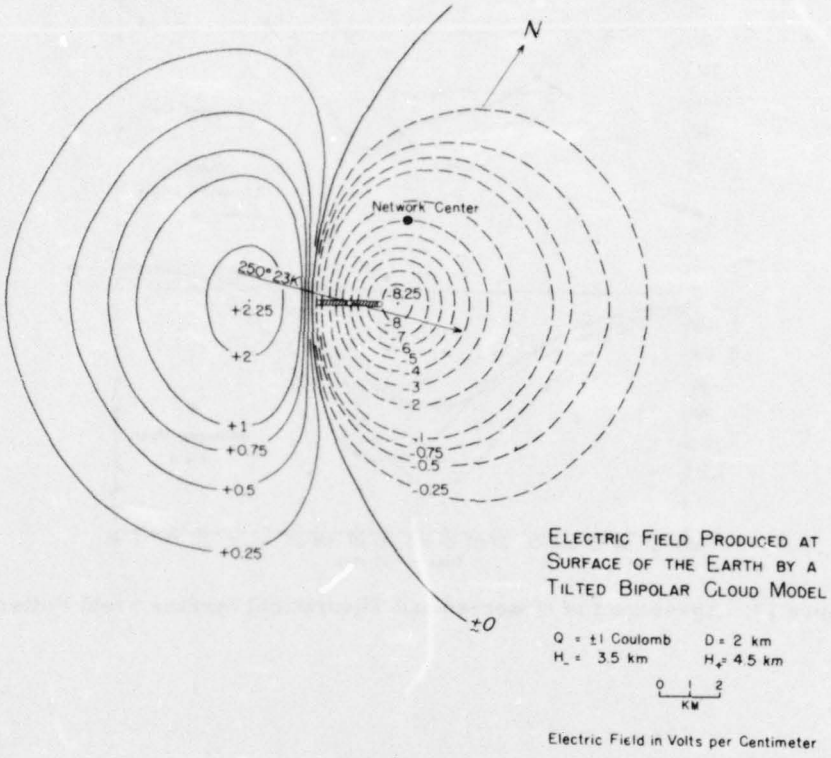

Figure 15. Tilted Dipole Field Pattern

The presence of in-cloud field breakdowns or lightning is seen primarily as a transient modulation of the quasi-static field pattern as it moves past a station. An example of these field changes during a weak thunderstorm passage is seen in Figure 16. Electrical activity in the storm would not have been noticed through conventional weather observations, since no lightning was observed. Such charged cloud structures may readily produce isolated lightning strikes to aircraft entering the cloud as will be seen in the following section.

More active propagating storm systems display short period intense positive and negative field alterations which maintain considerable pattern similarity as the charge concentrations move across a station network. A good example is shown in Figure 17.

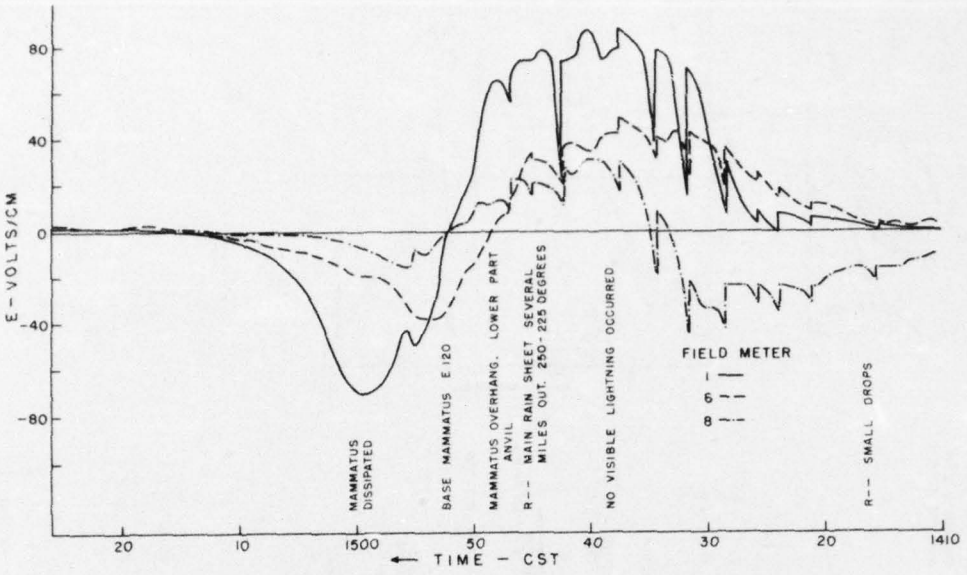

Figure 16. Surface Field With Nearby Weak Thunderstorms

3.3.2 STORM FLIGHT DATA

3.3.2.1 Clear Air Examples

Field measurements during clear air flight near the sides or above thunderstorms can be used to locate zones of increased storm lightning hazard. In flight, all three components of the electric field vector can be measured. Thus it is possible to construct a bearing to the centroid of charged elements contributing to the field. This direction will change along the flight path as the charged elements in the storm vary in intensity and location in response to the draft and precipitation time history at particular locations in the storm.

Illustrations of the field variations are given in Figures 18 and 19. Figure 18 depicts the two dimensional (Z, Y) field vector time-distance pattern during the C-130 take-off and early climb in the vicinity of a large nearby thunderstorm complex. Each vector indicates the direction to the left or right and above or below that a positive charge would move in the instantaneous electric field. The magnitude of the field is given by the length of the vector. The initial disturbance is the normal apparent field variation as the aircraft leaves the ground. Initial climb was under the main negative charge zone of the storm. The aircraft then turned and came out under the positively charged lower anvil region as shown by the vector reversal in direction.

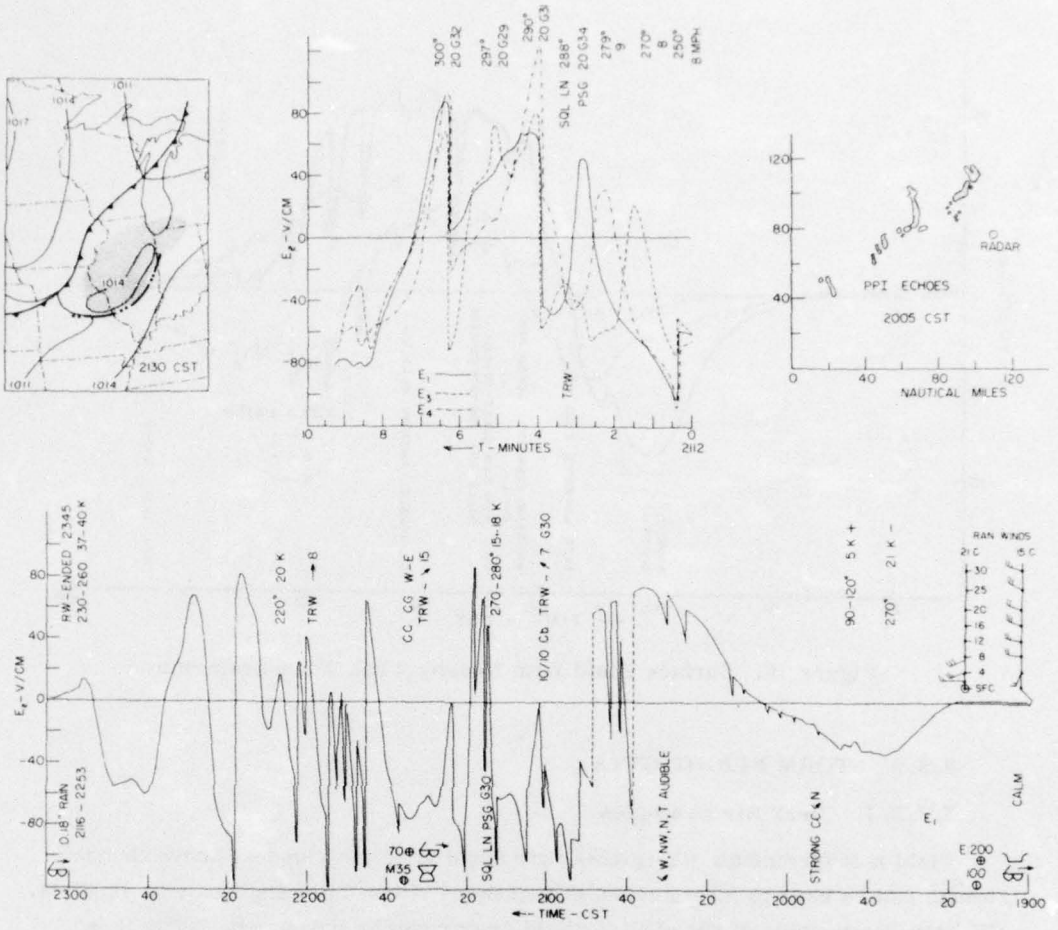

Figure 17. Surface Field With Active Storm

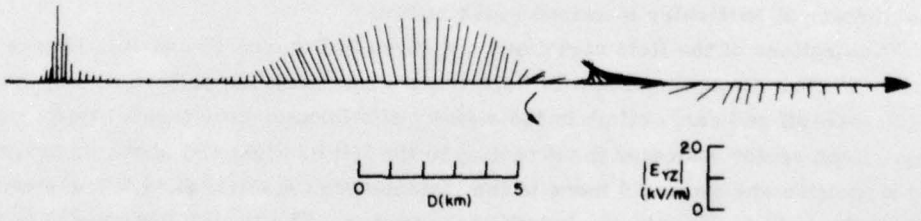

Figure 18. Low Altitude Field Variation Under Storm

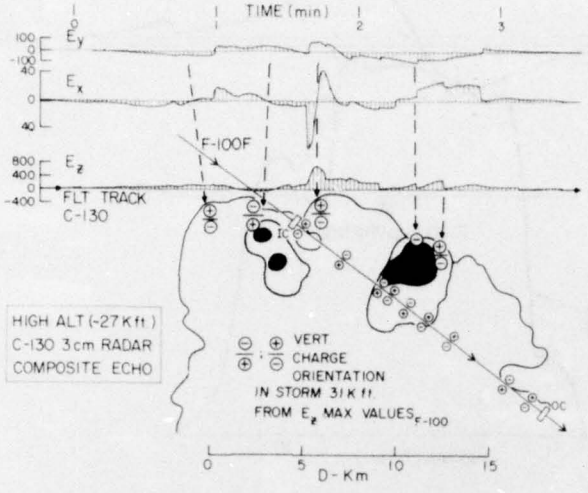

Figure 19. High Altitude Field Variation Alongside Storm

Flight at high altitude along the edge of a large thunderstorm is shown in Figure 19. It indicates a composite PPI radar cross-section constructed from the navigational radar data on the C-130 and the echo relation to the three external field components. It can be seen that field maxima in the vertical component (E_z) and the wing-span directed component (E_y) occur near the same times and near the zero cross-over point between the negative and positive maxima's of the flight-direction component (E_x). These zero crossovers in (E_x) represent approximate positions of centers of excess charge near the C-130 flight level and the maxima and minima in E_x are approximate boundaries of the most significant charge zones near the aircraft. In this case, southern, central, and northern charge concentrations are indicated from the clear air fly-by data and are generally confirmed by the more complicated structure found in the storm on the F-100F penetration.

U-2 data taken above storms usually indicates a pattern very similar to that shown in Section 3.3.1 for surface field disturbances under storms.

Figure 20 illustrates an apparently simple dipolar type oscillation observed on a pass above a small developing thunderstorm over the ocean. The F-100F entered the storm at 9 km shortly after this pass and triggered a lightning event in the center of the storm. Positive charge was removed from the vicinity of the F-100F and, as seen in the figure, negative charge was removed from the upper cloud region. On the subsequent pass, another lightning event was observed near the aircraft, this time positive charge was removed from the vicinity of both aircraft. By the final pass, the field at U-2 altitude had dropped to ± 3 kV/m although the field at F-100 altitude was still up to 40 kV/m peak values. No lightning was observed on this pass.

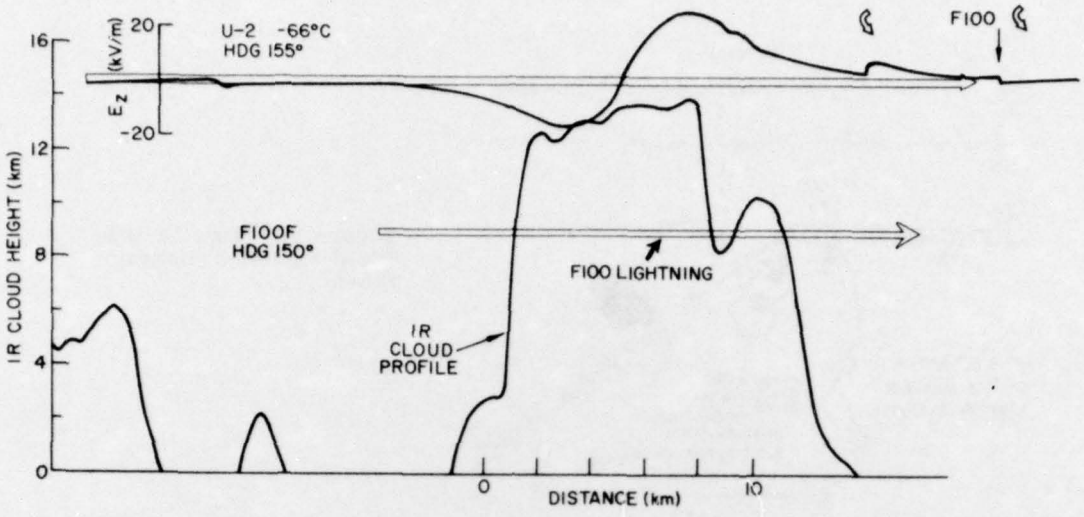

Figure 20. Field Variation on Over-Flight of Small Thunderstorm

The infrared sensor data for storm overflights has been used in conjunction with polynomial approximations to radiosonde soundings in the storm vicinity to calculate temperature height profiles for the storm tops. When proper account is taken of the normal airspeed variations that occur, it is possible to map a fairly accurate profile of the storm geometry. Figure 20 also illustrates the structure in relation to the field pattern. The newer, developing NW portion of the storm, reported by the pilot to be building rapidly, is seen to have excess positive charge below the U-2.

3.3.2.2 Storm Penetration Data

Interpretation of the complex field patterns observed within storms has required analysis of a number of passes at different altitudes and stages of storm development to unravel the details of the variations. The structure near 4.5 km altitude can be examined with reference to Figures 21 and 22. These illustrate relations of the vertical field component to the cloud liquid water content and precipitation features at this altitude. The C-130 followed the F-100F through a vigorous congestus cloud embedded on the southwest flank of an older thunderstorm mass on the first of these passes. Acceleration and draft data from the F-100F indicated the passes were more active than the average thunderstorm pass. The C-130 experienced up to 25 knot indicated airspeed fluctuations with pitch variations of about ± 5 deg from flight normal. The time-lapse color photography indicated the NE side of the P1 cloud was very dark. Heavy precipitation was encountered in the central downdraft area. It was followed by lighter cloud in the SW exit area.

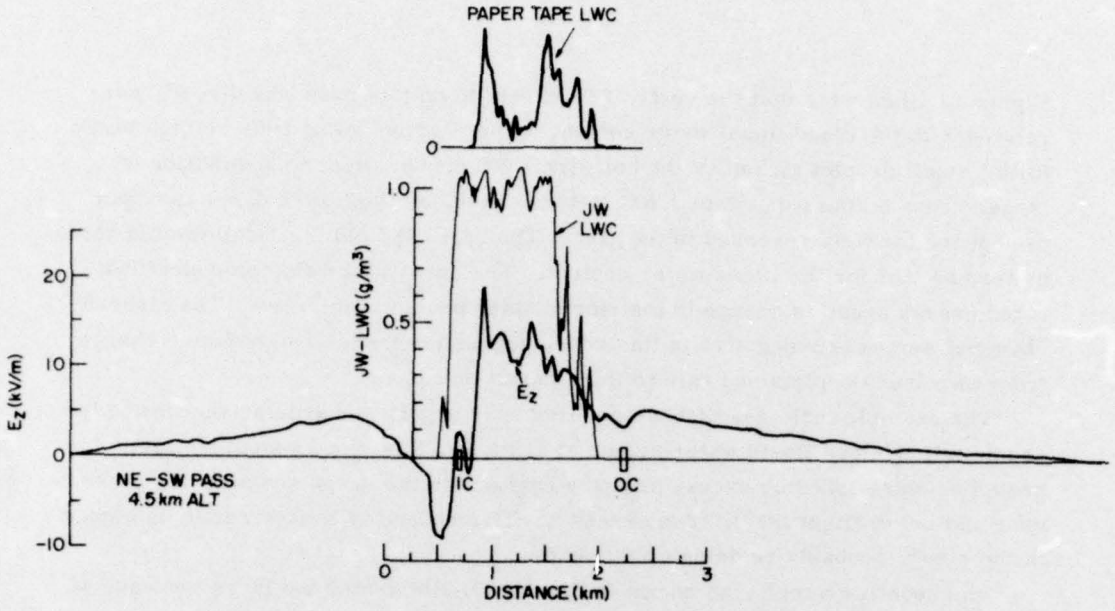

Figure 21. Electric Field and Liquid Water Content - Pass 1

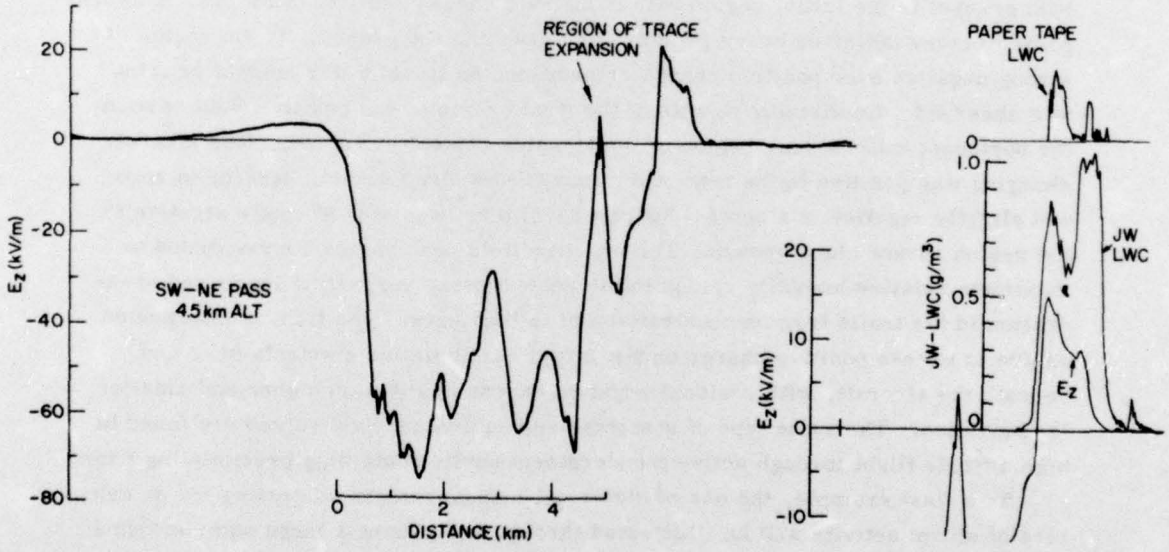

Figure 22. Electric Field and Liquid Water Content - Pass 2

Figure 21 illustrates that the vertical field profile on this pass was directly correlated with the cloud liquid water content. The negative going field relates to the initial small droplet pickup by the hot wire LWC probe, prior to acquisition of larger drops on the paper tape LWC meter. Then, as the larger droplets began to appear, the field reversed to positive. The vertical field trace follows the same pattern as that for the liquid water content. The horizontal field component indicated excess negative charge in the storm radar precipitation core. The aircraft charging was weakly negative in this zone, suggesting transfer of negative charge from the cloud droplets and rain to the aircraft on impact.

The example indicates that the positive over negative charge orientation in the precipitation/cloud liquid water region at 4.5 km in this cloud should be interpreted as established by excess negative charges on the drops and droplets present near and below flight level. The excess positive charge is considered to be higher in the cloud, probably residing on the snow.

The second example, as shown in Figure 22, illustrates the large increase of field and the field directional reversal accompanying the conversion of the cloud to solid precipitation forms. This pass from SW to NE was through snow showers with graupel in the initial region with some rain shower activity to the NE. Pictures prior to entry indicated heavy precipitation reaching the ground. In the region of strong negative over positive charge orientation, no liquid water content or icing was observed. Confirming results of the first example, the positive field zone in the northeast was the only region of liquid water content at 4.5 km. The aircraft charging was positive in the first snow shower downdraft region, tending to zero and slightly negative in a central updraft zone; then becoming strongly negative in the region of new cloud growth. The negative field peak values corresponded to maximum relative humidity values in the snow region, suggesting increased evaporation in the trails from concentrations of falling snow. The field is interpreted as due to excess positive charge on the larger precipitation elements near and beneath the aircraft, with residual negative excess charges on higher and smaller ice particles. The same type of structure and equivalent field values are found in high altitude flight through active thunderstorm anvils containing precipitating snow.

As a final example, the use of electrical measurements in locating major centers of storm activity will be illustrated through analysis of a large summer-time Florida thunderstorm aggregate located 40 to 50 nm SW of Patrick AFB. In deriving the data, numerous radar composite charts, aircraft flight tracks, and cloud photographs were prepared to establish the overall storm configuration. Three long N-S lines of cumulonimbus activity were present, with adjoining layers of altocumulus and stratocumulus at mid and lower altitudes. Extensive cirrus storm anvils and organized lines of cumulus and cumulus congestus were

associated with the storms. The cloud bases were near 1 km and the tops were about 14 km.

Detailed calculations of electric fields and cloud top infrared temperatures, were made for eleven U-2 passes over the storm. A summary of this data is given in Table 2. It should be noticed that large positive and negative field values were observed above the storms. A typical profile is seen in Figure 26. Storm penetrations were made by the F-100F at nominal 8.8 km pressure altitude. Six passes were made through the same general area of this storm. An additional four passes were made through nearby storms. Electric fields, accelerations, vertical relative wind, aircraft height changes and free air temperature were calculated for some of the passes. The aircraft received a strong lightning strike on the nose during the first pass through a radar cell measuring 15 km E-W by 25 km N-S. The U-2 cloud top measurements indicated 14 km to 14.2 km IR tops in this cell. Visible tops were probably 1 to 2 km above the IR tops since on the 5th pass the U-2 went through the edge of a plume extending to at least 14.9 km. The cell expanded and merged with other activity to form a WSR-57 radar echo 40 km E-W by 75 km N-S by the time of the fourth pass.

The penetration flight data are summarized in Table 3. The lightning strike on P1 resulted in a transient field change of -195 kV/m in the vertical field component, suggesting excess positive charge above the aircraft was removed in the strike. The cell at this time was in an early mature stage with strong updrafts present and a large warm thermal anomaly due to release of latent heat. The vertical field at flight level indicated a positive over negative charge orientation for most of the pass as can be seen in Figure 23, which shows relations between the field, vertical motion, and temperature for the pass. The E_z and E_y components have been corrected for roll and are shown in perspective fashion in Figure 24. Each vector origin is a position on the diagonal flight path. The vectors are in the E_y, E_z plane at each location and indicate the direction toward excess negative charge centroids. Pilot comments are also indicated. Detailed analysis suggests that this data may be interpreted as follows.

The initial plus over minus region was associated with excess positive charge in the lower region of a snowing anvil overhand. The field then became horizontal as the aircraft neared the congestus buildups to the right. As it entered the new northern growing side of the cell, negative over positive charge was found. This was a zone of intense concentration of small supercooled water droplets in a strong updraft. Further into the older storm region, mixed-phase precipitation was present in the draft with a positive over negative orientation, with the vectors indicating main precipitation area/radar cores below and to the right of the aircraft. The major sustained updraft area was toward the southern end of the cell in the region of maximum field vectors. New congestus buildup activity was found on the southern edge in the region of field reversal to negative over positive and in the new growing cloud area to the south.

Table 2. Summary of U-2 Data 9 August

Time Over Max Top HT (Z)	IR Max Top (km)	Field Maximums on Pass (kV/M) Max E_z+ (-below AC)	E- / E+	Max E_z- (+below AC)	Aircraft Radar Alt (km)	Dimension of Field Disturbance (km)	Dimension of IR Cloud Top abv 11 km on Pass (km)
1838:43	14.3	44	1.98	87	14.03	30	30
1842:45	14.5	35	1.69	59	15.68	52	48
1848:27	14.3	33	1.03	34	15.45	33	30
1850:20	14.2	25	0.32	8	15.54	33	28
1858:14	13.9	17	1.00	17	14.90	32	28
1914:08	13.9	32	1.22	39	15.67	51	43
1918:14 (1)	13.7	21	1.29	27	15.32	45	
1919:04 (2)					15.58		71
1921:50	13.6	8	0.88	7	15.80	32	
1927:01	13.6	40	1.23	49	15.50	50	70
1932:10	13.5	20	0.75	15	15.89	50	66
1938:30	13.5	35	1.06	37	15.07	55	51

Table 3. Summary of F-100F Data - 9 August - 1st Flt 8.8 km Pressure Alt.

Pass	Field Maximum On Pass (kV/m) Max $\lvert E_y \rvert$	Max $E_z(+)$	Max $E_z(-)$	E(+)/E(-)	Lightning Strike ΔE (kV/m)	Max AC Ht Change Meters	Max Updraft m/sec	Max Down-Draft m/sec	Mean Free Air Temp T-°C	Temp Perturbation °C
1	255	525	250	2.1	-1950	210	18	0	-29.5	6.2
2	240	550	300	1.8						
3	250	1200	800	1.5		MSG	MSG	MSG	MSG	MSG
4	240	450	500	0.9		160	15	8	-29.5	5.5
5	215	450	25	18					-30	1.7
6	235	450	400	1.1					-30	3.1
Other Storm Areas										
3C	235	375	400	0.9		MSG	MSG	MSG	MSG	MSG
4A	245	450	400	1.1		420	16	5	-30	3.5
4C	240	450	175	6		65	6	5	-30	2.3
7	240	300	350	0.9		170			-30.5	2.9

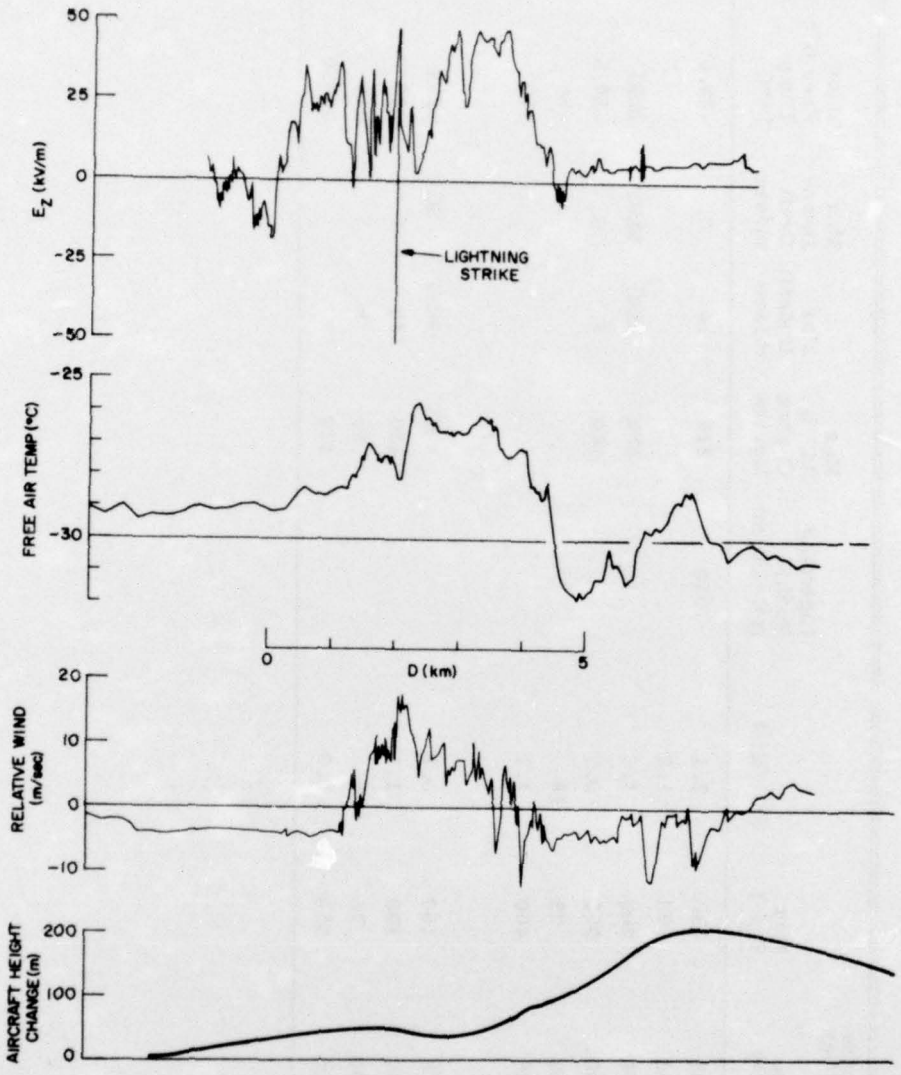

Figure 23. Electric Field, Draft, and Temperature - Pass 1

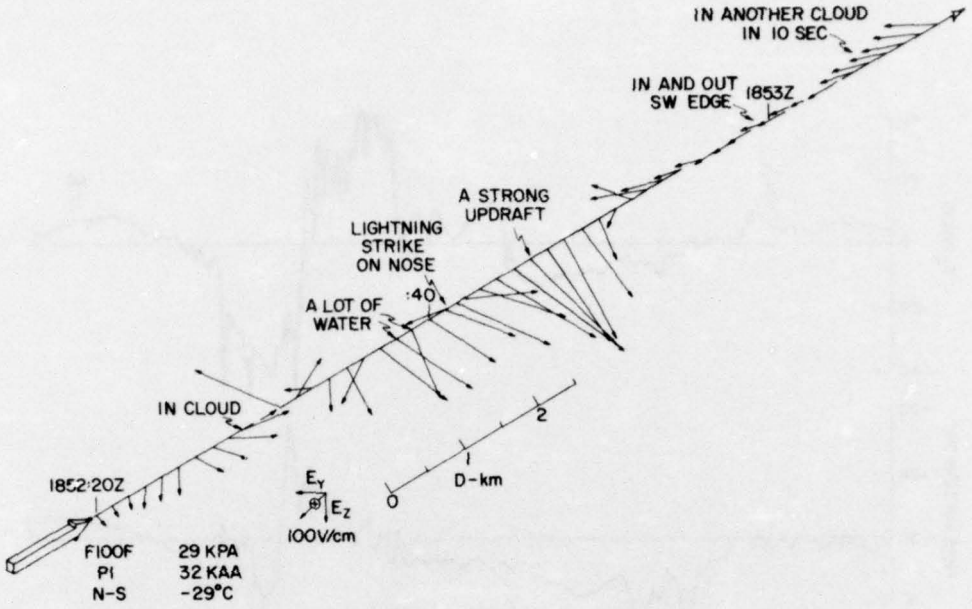

Figure 24. Electric Field Perspective - Pass 1

Another of the passes contained some particularly interesting examples of field correlations with storm structure that are illustrated in Figures 25 and 26.

Figure 25 indicates the observed relations of the vertical electric field, the air temperature, the relative vertical wind component, and the aircraft height change on a S to N pass. The $+E_z$ zone in the center of the cloud is seen to be primarily in a region of about 5 to 9 msec updraft and progressively warming air temperature. The sharp transition from positive to minus E_z occurs in the shear zone between up and down relative winds at a near zero draft velocity. The first peak negative field occurs in the central upward relative wind zone of about 7 msec. The field then tends in a positive direction from its negative peak of about -50 kV/m to about -20 kV/m with the thermal maximum of -26.5°C and the edge of the next downward relative wind zone. The field tends to increased negative values with the colder air at about -32°C and a near zero draft velocity. Two subsequent short duration negative peaks are seen to occur with sharp upward increases in relative wind on the edges of a 1.5°C warmer temperature anomaly.

The main features of this field pattern were also observed in the clear air above the storm. Figure 26 indicates the U-2 and F-100F field data, the infrared cloud top profile, and the radar cross-section intersections with the vertical plane containing the flight tracks.

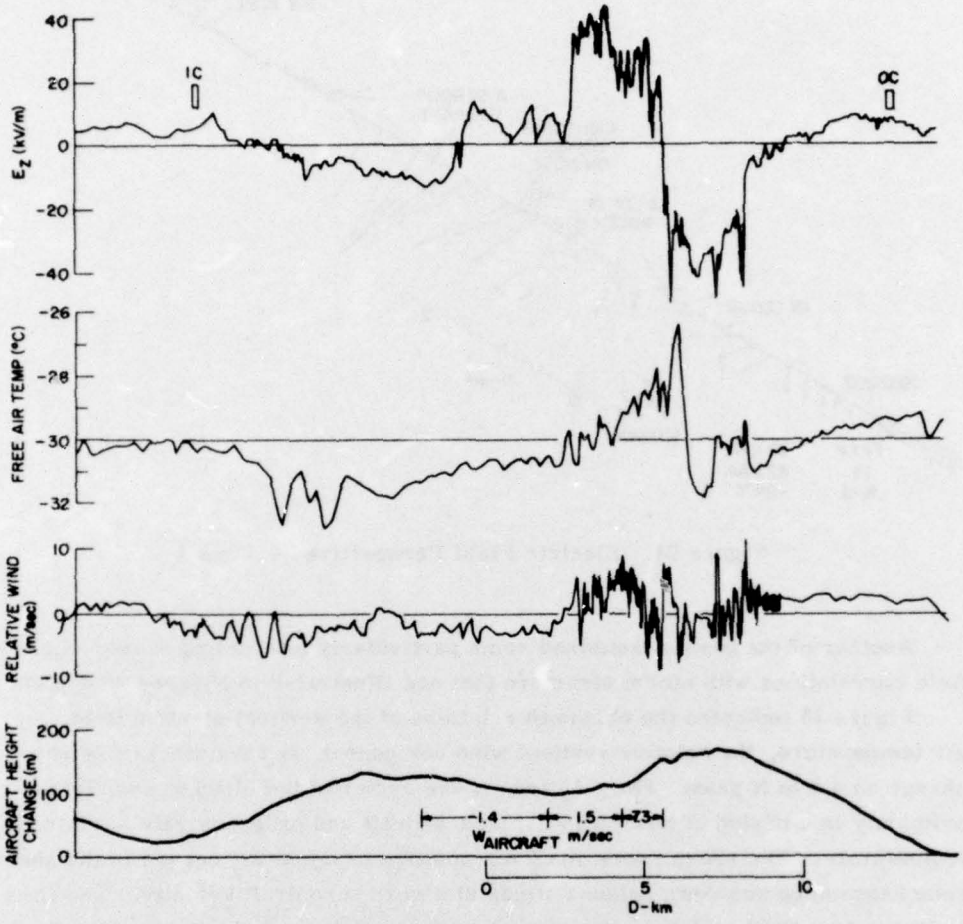

Figure 25. Electric Field, Draft and Temperature - Pass 4

It is seen that the main zero crossings and field maxima of the two patterns converge in the region of the principal radar echo core at high altitude and the center of the precipitation region shown on the Air Traffic Control radar. From Figure 25, it is also seen that this was the region of maximum thermal anomaly and turbulence encountered on the pass. The clear-air flyby data from the C-130 also indicated maximum electrical activity in this portion of the extensive cloud mass.

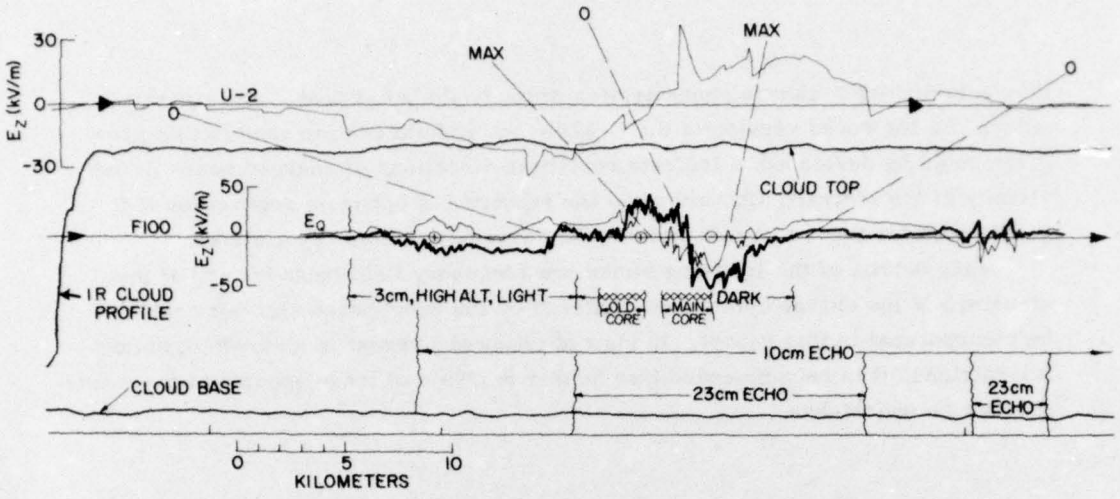

Figure 26. Cloud Geometry, Near-Simultaneous Electric Field In and Above Storm - Pass 4

4. CONCLUSIONS

It has been shown that properly located electric field sensors can be used to obtain realistic data within storms. The main features of such data correlate well with simultaneous observations taken outside the visible cloud boundaries. Thus when the in-storm field patterns have been properly related to the precipitation, draft and thermal patterns, it becomes possible to interpret the clear-air field structure in terms of probable in-storm conditions that would be encountered if a storm penetration were made at particular points along the field pattern.

Some of the complex relationships between storm parameters and electric fields have been illustrated. The field polarity and detailed development of a pattern observed at a particular altitude is directly related to details of the draft structure and to the local liquid/ice water content.

Lightning events were often associated with boundary zones between fairly small -200 to 500 m- regions of charge concentration. Penetration of large, fairly uniform, zones of 50 to 100 kV/m fields associated with precipitating snow normally did not result in lightning events. It appears that the localized charge singularities established by the small-scale motions and precipitation patterns are of most importance in the aircraft-triggered lightning phenomena. These zones may persist for 10 to 20 min after the generating processes in the area have ceased.

Some of the lightning/static discharge events to normal commercial and military flights may be associated with these zones. If the normal cloud penetration airborne radar technique of going through a present weak-echo region is used, it should be noted that this region may have been a previous active storm region,

thus establishing a charge concentration which could break down upon aircraft entry. An improved version of the C-130 electric field system used in this program could be developed to indicate real-time directions of charged zones in the vicinity of the aircraft, thus aiding in the selection of optimum regions for IFR penetration for those aircraft that may be adversely affected by a strike.

Many details of the lightning strike low frequency field behavior and of the structure of the charge centers encountered by the penetration aircraft could not be incorporated in this report. In view of renewed interest in aircraft-lightning interactions, it is recommended that further analysis of these aspects of the existing data be undertaken.

References

1. Byers, H.R. and Braham, R.R. (1949) The Thunderstorm, U.S. Govt. Printing Office, Washington, D.C.

2. Gunn, R., et al (1946) Army-Navy precipitation static project, Proc. Inst. Radio Eng. 34:156 and 34:234.

3. Chapman, S. (1955) Discharge of Corona Current from Points on Aircraft or on the Ground, Report CAL66. Cornell Aeronautical Laboratory, Inc., Buffalo, N.Y.

4. Clark, J.F. (1957) Airborne measurements of atmospheric potential gradient, J. Geophys. Res. 62:617.

5. Fitzgerald, D.R. (1965) Measurement techniques in clouds, in Problems of Atmospheric and Space Electricity, ed. S.C. Coroniti, Elsevier Publishing Co., Amsterdam.

6. Fitzgerald, D.R. (1967) Probable aircraft triggering of lightning discharges in certain thunderstorms, Mo. Wea. Rev., 95:835.

7. Fitzgerald, D.R. (1968) USAF flight lightning research, in Proc. Conf. on Lightning and Static Electricity, 3 to 5 Dec 1968. AFAL TR-68-0290, DDC - AD 693135.

8. Fitzgerald, D.R. (1970) Aircraft and rocket triggered natural lightning discharges, in Proc. Lightning and Static Electricity Conf., Soc. of Auto Engrs, N.Y.

9. Fitzgerald, D.R. (1974) Electrical structure of large overwater shower clouds, in Electrical Processes in Atmospheres, ed. by H. Dolezalek and R. Reiter, Dietrich-Steinkopff, Darmstadt, Germany (in press).

10. Fitzgerald, D.R. and Cunningham, R.M. (1965) Multiple aircraft studies of the electrical properties of thunderstorms, in Proc. Intl. Conf. on Cloud Physics, Tokyo and Sapporo, Japan.

11. Waddel, R.C. (1948) An electric field meter for use on airplanes, Rev. Sci. Instr., 19:31.

12. Mapleson, W.W. and Whitlock, W.S. (1955) Apparatus for the accurate and continuous measurement of the earth's electric field, J. Atmos. Terr. Phys. 7:61.

13. Kasemir, H.W. (1951) Die Feldkomponentenmuhle Tellus 3:240.

14. Kasemir, H.W. (1964) The Cylindrical Field Mill, US Army Electronics Command, TR ECOM-2526, Fort Monmouth, N.J. (DA Task No. 1VO-14501-B-53A-11).

15. Fitzgerald, D.R. (1957) Some theoretical aspects of the relation of surface electric field observations to cloud charge distributions, J. Met., 14:505.